Lithium isotopic fingerprints of sources and processes in surface waters of the Ebro River Basin (Spain)

Philippe Négrel, Romain Millot

Lithium isotopic fingerprints of sources and processes in surface waters of the Ebro River Basin (Spain).

Philippe NÉGREL[1], **Romain MILLOT**

BRGM, F-45060 Orléans, France.

Abstract

The Ebro River in north-eastern Spain is among the largest contributors of freshwater to the Mediterranean Sea and ends in the Ebro delta, one of the major wetlands in Europe. The bedrock of the Ebro River basin mainly consists of carbonate rocks and evaporites of Paleozoic and Mesozoic age, and the river flows through several large cities, and agricultural and industrial areas. The Ebro River outlet at Amposta was sampled once a month for a year (2006), and a field campaign in April of the same year sampled the Ebro along its main course as well as its principal tributaries. In the present study, the behaviour of Li and its isotopes was investigated at basin scale, with the objective of elucidating the processes controlling the isotope signatures of a large river draining mostly sedimentary bedrock. δ^7Li values ranged from +17.1‰ to +18.3‰ along the Ebro main stream, and between +16.3 and +18.9‰ at the outlet. In the major tributaries, the δ^7Li values ranged from +12.9‰ to +20.9‰, with bedrock values ranging from +0.5 to +29.3‰. Comparing Li concentrations with Cl and SO_4 ones, it appears that evaporite weathering plays an important role in controlling Li, but no anthropogenic agricultural or industrial influence on Li concentrations was detected. The Na/Li, Cl/Li and SO_4/Li ratios clearly reflect the role of halite dissolution for some tributaries (Gallego, Ega and Aragon), gypsum dominating others (Guadalope, Matarrana, Huerva and Segre), and little influence of carbonate in all tributaries, the Ebro itself being a mixture of all tributaries. We tentatively applied the simple Rayleigh fractionation model, but most δ^7Li values of the Ebro water samples plotted away from the fractionation line, reinforcing the major role of mixing processes in the Ebro basin, rather than fractionation processes during water/rock interactions. A comparison of δ^7Li values and $^{87}Sr/^{86}Sr$ ratios further demonstrates the role of gypsum/anhydrite and limestone in the Ebro and its tributaries. Sr-isotopes show a non-negligible role of carbonate dissolution, generally considered to be weak in the control of the lithium cycle in catchments.

Keywords: Ebro River, Li isotopes, dissolved load, evaporite, carbonate

[1] Corresponding author at: 3 Avenue Claude Guillemin, BP6009 - 45060, Orléans cedex 1, France.
E-mail address: p.negrel@brgm.fr (Ph. Négrel).

1 – Introduction

Lithium is one of the modern tools for studying water-rock interaction processes. This is done by coupling geochemical processes during such processes, with the capability of lithium to go into the fluid phase with significant mass-dependent fractionation between the two stable isotopes ^{6}Li (natural abundance 7.5%) and ^{7}Li (natural abundance 92.5%) (Huh et al., 1998, 2001; Pistiner and Henderson, 2003; Rudnick et al., 2004; Kisakürek et al., 2004; Pogge von Strandmann et al., 2006, 2014, 2021; Millot et al., 2007, 2010a, b; Négrel et al., 2012; Dellinger et al., 2014; 2015; Henchiri et al., 2016; Négrel and Millot, 2019; Qi et al., 2019; Martin et al., 2020; Steinhoefel et al., 2021; Millot and Négrel, 2021). Recently, the variation in $\delta^{7}Li$ values of water was used for distinguishing between natural and anthropogenic inputs because lithium isotopes have been shown to be a probe for tracing anthropogenic activity (Choi et al., 2019; Négrel et al., 2010, 2019; Millot and Négrel, 2021).

Lithium and its isotopes are of increasing interest in weathering studies through rivers dissolved and suspended loads and groundwaters because Li is solubilized from minerals and rocks during water–rock interactions (e.g. a mobile element) and not constrained by biological processes. Such chemical weathering induces isotopic fractionation resulting in an enrichment of the heavy isotope (7Li) in solution, the light isotope (6Li) being preferentially retained in secondary weathering mineral phases (see Négrel and Millot (2019) and references therein). In systems where few secondary phases are formed, lithium can evolve in terms of a tool tracing the mixtures between waters (see Négrel et al. (2010) and references therein).

The weathering of silicate rocks is a major process at the earth's surface and to better understand this process, many studies have deployed the use lithium isotopes(e.g., Burton and Vigier, 2011; Steinhoefel et al., 2021 and references therein). However, carbonate and evaporite weathering processes have hardly been studied through Li-isotope variations (Gou et al., 2019; Martin et al., 2020). This can be explained by two features: i) Li contents in

evaporite and carbonate are low (<12 µg g^{-1}) compared to silicate rocks (20-40 µg g^{-1} in granite and around 60 µg g^{-1} in shales); and ii) the most common rock types in Europe are 39% plutonic and metamorphic rocks, 37% shales, 14% carbonate rocks, 9.5% sand-sandstones, and volcanic rocks and evaporites playing a subordinate role (Caritat and Reimann, 2012).

Here, we focus on Li-isotope data from the dissolved load of 25 river-water samples collected in the Ebro Basin and of 2 groundwater samples. Among the rivers providing freshwater in the Mediteranean Sea, the 2017 Mediterranean Quality Status Report (downloaded at https://www.medqsr.org/fr/node/230 on February 2023, 14th) classified the rivers having their outlet in the Mediterranean through their annual climatological discharge of freshwater in cubic metres per second. The Rhone and Po rivers have the highest discharge (1500-1800m^3/s), then the Nile (1000-1500m^3/s) followed by the Ebro and the Drin with 500-1000m^3/s, reflecting the importance of the Ebro in the hydrologic cycle of the Mediterranean Sea. The last rivers supplying the Mediterranean are the Ceyhan, the Evros and the Tiber (150-500m^3/s) and the Moulouya and Shellif (10-150m^3/s). We measured lithium and its isotope values in all reservoirs, in parts of the basin affected by salinization and secondary processes (precipitation, re-dissolution, mixing of water and anthropization), as well as in the main bedrocks. Studies on river drainage basin having evaporite-type bedrocks are scarce and in these cases, the evaporitic deposits are often located in headwaters and are not very important in terms of surface area compared to the general geology (mainly silicate rocks) and to the size of these of large river basins. The δ^7Li values generally observed in rivers draining evaporites are either around +20 ‰ (Huh et al., 1998; 2001; Gou et al., 2019; Yoon, 2010) but other rivers also influenced by evaporite dissolution have low δ^7Li values, around +8‰ (Chen et al., 2002; Chetelat et al., 2008, 2009; Wang et al., 2015; Ma et al., 2020), whereas carbonate-dominated rivers are characterized by high δ^7Li values (> +20‰). The objectives

of our study were to constrain the Li cycling in a major river basin underlain by sedimentary rock and affected by climatic impact (drought and water deficit), and to examine Li in the rock-soil cycle through weathering processes and water use (agriculture, water reservoirs and industry), again within a climate-change context.

2 - Characteristics of the Ebro Basin

The Ebro River basin (Fig. 1) lies in north-eastern Spain, starting near the Atlantic coast in the Cantabrian Mountains and flowing to the western Mediterranean Sea. Over its 85,530 km² drainage basin and along its 928-km course, the Ebro River flows through several large cities (Lleida, Logroño, Vitoria, Zaragoza, Huesca and Barcelona), and through agricultural, mining and industrial areas. It is the largest Spanish river system and one of the largest contributors of freshwater to the Mediterranean Sea (CHE, http://www.chebro.es/).

The geology of the Ebro Basin consists of (Guillén and Palanques, 1992; Luzón et al., 2008; Mochales et al., 2007) sedimentary and metamorphic Palaeozoic rocks (Iberian and Pyrenees mountains, Priorat Massif); Jurassic and Cretaceous carbonate rocks in the Iberian Chain forming the southern margin of the Ebro Basin; sedimentary Tertiary rocks of the Pyrenees foothills and the Ebro Valley; and Neogene and Recent delta-plain deposits near the Mediterranean Sea (lower part of the Ebro River). The occurrence of evaporite deposits in the Ebro River basin has been documented in detail (Castillo Herrador, 1974; Birnbaum, 1976; Ortì, 1990; Utrilla et al., 1992; Elorza and Santolalla, 1998).

The main tributaries of the Ebro are the Aragon, Gallego, Cinca and Segre rivers (northern part of the basin, Fig. 1) flowing through silicate rocks of the Pyrenees Mountains in their upper part, and through sedimentary rocks downstream. In the southern part of the basin, the main tributaries are the Huerva, Guadalope and Matarrana (Fig. 1), flowing over sedimentary rocks. The catchment of the Ega River, a tributary in the upper part of the basin, consists of sedimentary and metamorphic Palaeozoic and Mesozoic rocks of the Iberian

Chain. The four described climatic areas in the Ebro Basin (Batalla et al., 2004) are the Atlantic headwaters (annual average precipitation about 900 mm and contribution to runoff 23%), the west-central Pyrenees (950 mm, 31%), the eastern Pyrenees (800 mm, 41%) and the southern Mediterranean zone (500 mm, 5%), with a mean annual runoff of approximately 6837.10^6 m^3.

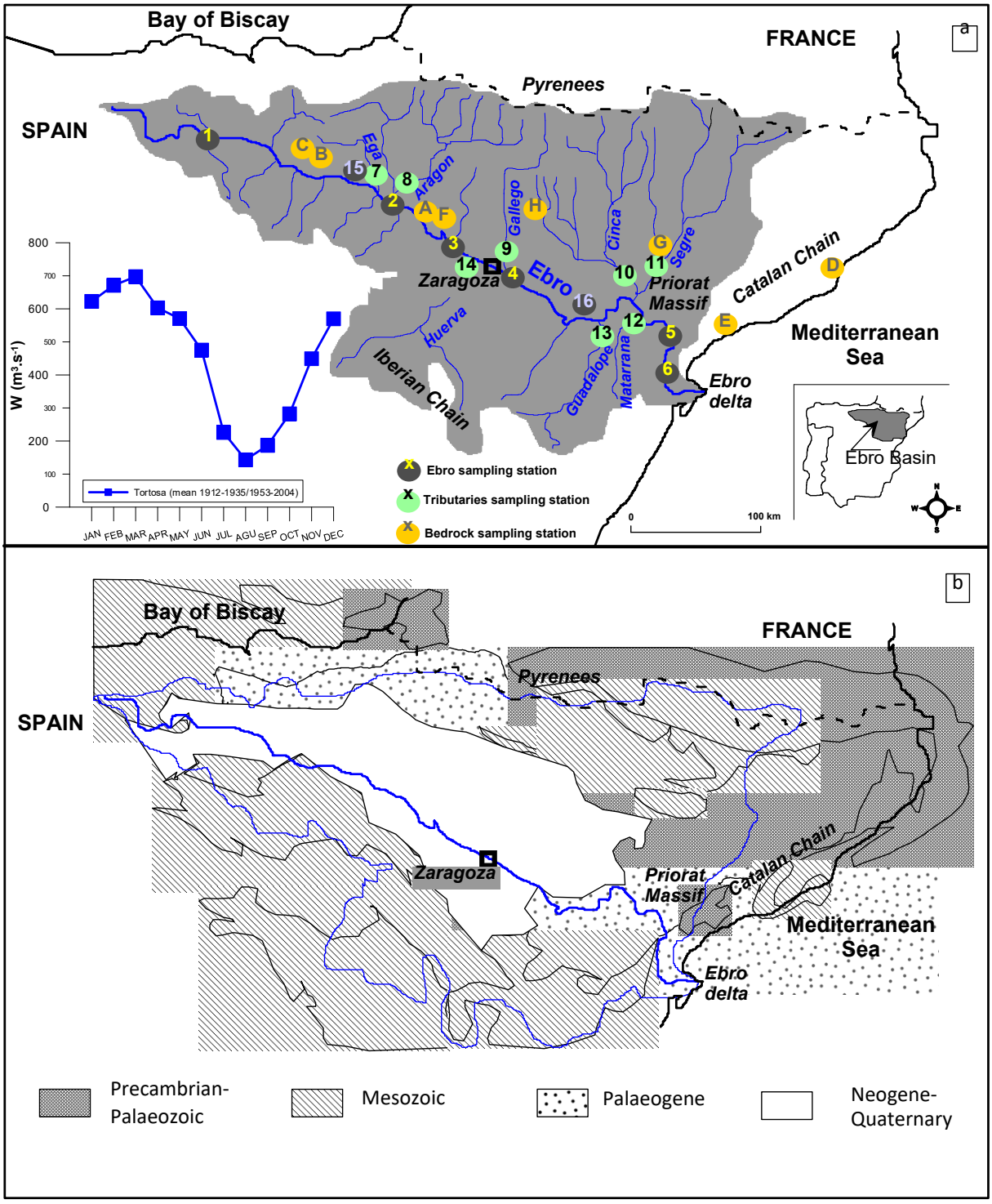

Figure 1. a- General location of the Ebro basin in Spain, location of sampling points in the Ebro Basin. The main river was sampled upstream and downstream from the confluences of the main tributaries, numbers 1 to 5 (number 5 being Tortosa); the tributaries were sampled at numbers 7 to 14. The Ebro outlet at Amposta (number 6; Cruzado et al., 2002) was sampled each month between June 2005 and May 2006. Groundwater was also sampled at two locations in the Ebro Basin (number 15 Andosilla in Navarra; irrigation well at 6-m depth, and number 16 Lleida; irrigation well at 7-m depth). Long-term evolution of the mean monthly discharge of the Ebro river in Tortosa (number 5,

modified from Négrel et al., 2007). b- Geological sketch map of ythe Ebor Basin, modified from Luzón et al., 2008 and Mochales et al., 2007).

The discharge of the Ebro River decreased from around 590 m^3 s^{-1} in the "natural" period 1914-1935, by 28% to 430 m^3 s^{-1} in the period 1960-1990 because of increased water use for irrigation, reservoir storage and electricity production, and domestic consumption (CHE, 1996; Ibáñez et al., 1996). The main water use is for irrigation with almost 700,000 irrigated hectares (total water demand of 6310 Hm^3 y^{-1}, CHE, 1996; INE, 2003), causing a huge hydraulic deficit. Nearly 60% of the surface area of the Ebro River Basin is covered by agricultural land, and around 50% of Spain's electricity is provided by hydroelectric power plants along the Ebro system, causing another deficit. Around 14% of land use concerns urban areas and industry, mainly located in the valleys.

More information on dissolved and suspended matter fluxes and weathering processes can be found in the different investigations we have conducted in the Ebro River catchment several, studying fluxes of (Négrel et al., 2007, 2016, 2021; Petelet-Giraud and Négrel, 2010).

3 – Material and methods

3.1. Water and rock sampling

The Ebro River and its main tributaries were sampled in the centre of each river channel from bridges (April 2006, Fig. 1). The main channel (samples 1 to 5, Fig. 1) was sampled upstream and downstream from the confluences of the main tributaries (7 to 14, Fig. 1). In order to monitor compositional variations over time in the river flow, the Ebro outlet at Amposta (6, Fig. 1; Cruzado et al., 2002) was sampled each month between June 2005 and May 2006. To provide an idea of the geochemical signature of potential groundwater input to surface water, two groundwaters were also collected (15, Andosilla in Navarra; irrigation well G15 at 6-m depth; and 16, Lleida; irrigation well GA-2 at 7-m depth). Representative gypsum, anhydrite

(4 samples) and carbonate (4 samples) bedrock samples were collected along the Ebro as well (Fig. 1, A to H; Table 1), halite is from University collection.

Table 1: Rock type (gypsum, anhydrite and carbonate), sample ID, sampling station locations and deposit type, δ^7Li and Li content for the different bedrocks. Na and Sr contents, $^{87}Sr/^{86}Sr$ ratios are from Négrel et al., 2021.

Type	Reference	Samples	Deposits	δ^7Li	Li	Na	$^{87}Sr/^{86}Sr$	Sr
					mg g^{-1}	mg g^{-1}		µg g^{-1}
gypsum	A	ABI-2	Miocene continental deposits	0.5	8.8	0.1	0.70818	2892
gypsum	B	MN14	Oligocene continental deposits	4.1	1.7	0.6	0.70830	2499
anhydrite	C	S3	Eocene marine deposits - Navarrese Potash Basin	13.6	9.2	2.7	0.70781	4590
anhydrite	D	TRIAS	Trias (Keuper) deposits	29.3	11.3	0.4	0.70766	2379
carbonate	E	S3 5.50m	Trias (Muschelkalk) limestone	12.6	3.4	0.7	0.70872	120
carbonate	F	ABC-4	Miocene continental deposits	17.7	7.7	1.2	0.70822	1035
carbonate	G	SA-40	Paleocene continental Garumnian facies	0.9	3.7	0.4	0.70779	511
carbonate	H	LFr2 14	Oligocene facies	15.3	1.4	0.8	0.70918	571
halite	Halites	HALITE	university collection	-	0.3	-	0.70864	2

3.2 Methods

After collection, the water samples were filtered through pre-cleaned 0.45 µm acetate filters; 100 mL was acidified with double-distilled nitric acid to pH around 2 and stored in pre-cleaned polyethylene bottles for major-cation analyses, and a further 100 mL was stored unacidified in polyethylene bottles for anion analysis. The water samples were analysed by ion chromatography for major ions, and by ICP-AES for Ca, Na, K, Mg and ICP-MS for trace elements (accuracy 5-10%) using protocols under accreditation. External and in-house standards as well as reference materials was used to calibrate and validate the values. Alkalinity was determined by the Gran titration method. We used HCl acid to titrate beyond the equivalence point. The quantity of acid added to the pH around 3 is used to determine this equivalence point with a mathematical method

Lithium-isotopic compositions (Millot et al., 2004) were measured with a Neptune Multi-Collector ICP-MS (Thermo Fisher Scientific). Chemical separation of lithium from the matrix before mass analysis used cationic resin (BioRad AG® 50 W-X12, 200–400 mesh)

and HCl acid (0.2 N) for 30 ng of lithium. Blanks for total chemical extraction were less than 20–30 pg Li, which is negligible as it represents a 10^{-3} blank/sample ratio. The $^{7}Li/^{6}Li$ ratios were normalized to a $\delta^{7}Li$ determination of about 0.1–0.2‰ (2σm). Accuracy and reproducibility of the total method (purification procedure + mass analysis) were tested by repeated measurement of a seawater sample (IRMM BCR-403) after separation of lithium from the matrix, for which we obtained a mean value of $\delta^{7}Li$=+30.8‰ ± 0.4 (2σ, n=15) over the duration of the analyses. This mean value agrees with our long-term measurements ($\delta^{7}Li$=+31.0‰ ± 0.5, 2σ, n=30).

4 – Results

Table 1 contains all analytical results for the different bedrocks and Table 2 contains data for the river water and groundwater.

4.1. Bedrock

The highest lithium content is observed in Trias-Keuper D anhydrite with a maximum around 11.3 µg g^{-1}, whereas the Oligocene B gypsum and Oligocene H carbonate have low lithium contents (about 1.4 to 1.7 µg g^{-1}). The $\delta^{7}Li$ ranges from +0.5 to +0.9‰ for the lowest values, observed in Miocene A continental gypsum (Li content about 8.8 µg g^{-1}) and in Paleocene G continental carbonate (Li content about 3.7 µg g^{-1}), up to +29.5‰ in Trias-Keuper D anhydrite and a highest Li content of around 11.3 µg g^{-1}.

4.2. Tributaries, Ebro main channel, and outlet survey

The eight sampled tributaries of the Ebro River (Fig. 1) show a minimum Li content of around 12 µg l^{-1} in the Rio Aragon and a maximum value of 66.9 µg l^{-1} in the Rio Guadalope. The δ^7Li value ranges from +12.9‰ in Rio Matarrana to +20.9‰ in the Rio Cinca.

Table 2: Sample ID, distance to Ebro source, river discharge ([CHE]), δ^7Li and Li content for surface water (Ebro survey at the Amposta station, Ebro main channel, tributaries, Fig. 1) and groundwater (Fig. 1) in the Ebro River Basin. Na and Sr contents, and $^{87}Sr/^{86}Sr$ ratios are from Négrel et al., 2021.

Samples	Station	Sampling date	Distance to the source	Discharge	δ^7Li	Li	$^{87}Sr/^{86}Sr$	Sr	Na
			km	$m^3\ s^{-1}$	‰	µg L^{-1}		µg L^{-1}	µg L^{-1}
Ebro survey Amposta Station									
jun.	E6	6/15/2005	552	150.7	17.4	13.3	0.70847	1150	65
jul.	E6	7/15/2005	552	141.6	17.3	15.4	0.70848	1370	77
Aug.	E6	8/11/2005	552	119.0	17.7	16	0.70854	1759	141
Sep.	E6	9/20/2005	552	124.5	17.7	23.3	0.70859	2437	171
Oct.	E6	10/10/2005	552	118.3	18.9	28.3	0.70854	2488	239
Nov.	E6	11/14/2005	552	120.8	18.3	35.8	0.70857	2660	245
Dec.	E6	12/21/2005	552	300.0	17.6	32.8	0.70844	2490	142
Jan.	E6	1/17/2006	552	402.3	17.5	23.2	0.70841	1940	97
Feb.	E6	2/15/2006	552	173.0	17.6	17.9	0.70850	1540	84
Mar.	E6	3/14/2006	552	452.0	16.3	13.6	0.70842	1180	65
Apr.	E6	4/19/2006	552	202.1	17.9	15.2	0.70849	1250	69
May	E6	5/22/2006	552	225.3	17.3	12.5	0.70858	1120	55
Ebro main stream									
Miranda	E1	04/18-20-2006	104	-	17.1	5.3	0.70864	704	48
Lodosa	E2	04/18-20-2006	241	68.2	18.3	6.9	0.70856	855	42
Gallur	E3	04/18-20-2006	281	97.1	16.7	16.6	0.70837	1440	96
Presa de Pina	E4	04/18-20-2006	336	105.9	16.2	23.5	0.70842	1850	138
Tortosa	E5	04/18-20-2006	543	138.0	16.5	14.7	0.70849	1270	70
Tributaries									
Ega	E7	04/18-20-2006	216	7.8	15.4	16.3	0.70807	1210	128
Aragon	E8	04/18-20-2006	233	9.4	13.9	12	0.70814	973	88
Galliego	E9	04/18-20-2006	328	2.6	19.0	20.7	0.70861	1750	223
Huerva	E10	04/18-20-2006	324	-	20.2	40.9	0.70862	3200	101
Guadalope	E11	04/18-20-2006	397	80.9	17.1	66.9	0.70786	5090	68
Matarrana	E12	04/18-20-2006	457	3.8	12.9	14.8	0.70796	1280	21
Cinca	E13	04/18-20-2006	422	0.2	20.9	20.7	0.70877	1550	118
Segre	E14	04/18-20-2006	422	3.0	18.9	16.2	0.70897	1840	53
Groundwater									
G15	E15	04/18-20-2006	200	-	17.4	126	0.70840	7400	732
GA-2	E16	04/18-20-2006	370	-	18.1	21.1	0.70847	3020	262

Similar to other studies of downstream and/or seasonal changes of lithium isotope ratios in river systems (Farber et al., 2004; Manaka et al. 2017; Pogge von Strandmann et al., 2017), we present their variation along the Ebro. Samples were collected from 100 km downstream of the river source to nearly the outlet, 450 km downstream.. The Li contents in tributaries, the main channel and the sampling-location distance from the source are plotted on Figure 2a, and the δ^7Li values on Figure 2b.

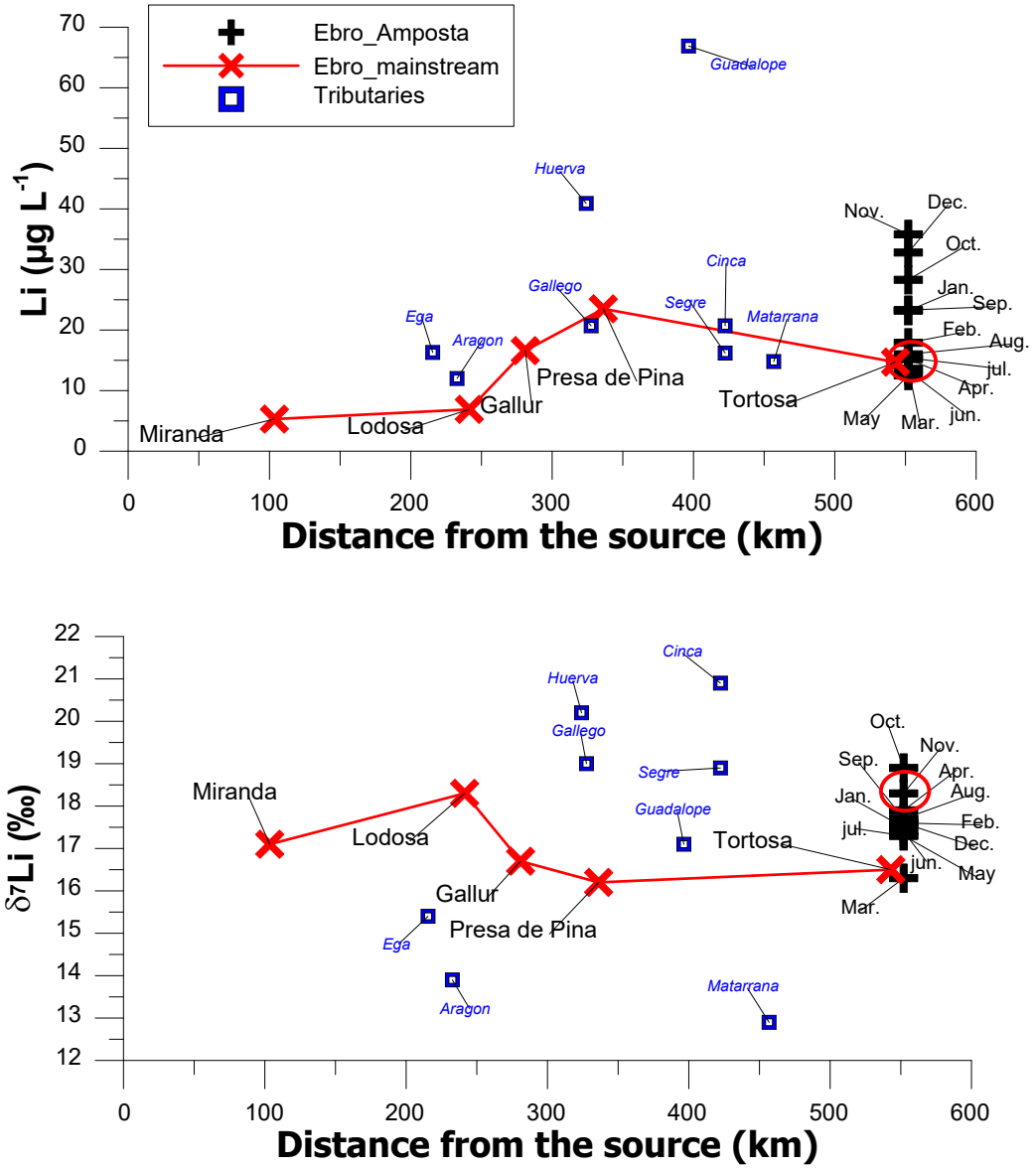

Figure 2a, b. (a) downstream variation of the Li concentrations (µg L^{-1}) and (b) δ^7Li (‰) values with distance from the source (0 km) to the outlet (500 km) for the Ebro main channel and tributaries. The variations at the outlet (Amposta, number 6 in Fig. 1a) are plotted with their sampling month; the red circle marks the Amposta sampling at the same time as the Ebro main-stream sampling.

The Li content in samples collected along the Ebro increases from 5 µg L^{-1} farthest upstream, to 23 µg L^{-1} 350 km downstream, and then decreases to 15 µg L^{-1} just before Amposta. During the survey in Amposta, Li contents varied between 12 µg L^{-1} in May and 36 µg L^{-1} in November. The δ^7Li values along the main channel increased slightly from +17.1‰ in Miranda de Ebro up to +18.3‰ in Lodosa and then, until Tortosa, remained

223 invariant around +16.5‰ (Fig. 2b). At Amposta, the δ^7Li value ranged between +16.3 and
224 +18.9‰. Please note the difference between the δ^7Li values in Amposta and Tortosa (a few
225 km upstream), whereas Li contents remained similar. This agrees with the discrepancies noted
226 for the $\delta^{44}Ca_{SW}$ and Ca contents in the same sample set (Négrel et al., 2021). This difference
227 may be related to the fact that these isotopic systems are sensitive to fractionation processes
228 (Dellinger et al., 2015; Négrel et al., 2020; 2021), and to the presence of dams between
229 Tortosa and Amposta increasing fractionation (Gou et al., 2019), both factors influencing the
230 isotopic values. Concerning the dams, their physical role is the retention and release of water
231 stocks. Depending on the periods of filling and emptying, the water stocks have different ages
232 as shown by Négrel et al., (2016) using H-O isotopes of the water molecule. These filling -
233 emptying processes must affect the isotopic values of chemical elements like calcium and
234 lithium which are subject to fractionation processes.
235 The PHREEQ-C code (Parkhurst and Appelo, 1999) allows to calculate the
236 distribution of aqueous species in water samples and the saturation index for minerals based
237 on the water data (e.g. the temperature, pH, redox and the concentrations of chemical
238 elements) and using the database of the thermodynamic parameters of the minerals (e.g. the
239 most recent Lawrence Livermore National Laboratory LLNL database). None of the water
240 samples in the Ebro Basin were undersaturated with respect to gypsum and anhydrite when
241 calculated with PHREEQ-C."Additionally, water samples of the tributaries and the Ebro were
242 systematically supersaturated for calcite, aragonite and dolomite. Samples from Amposta
243 showed various saturation degrees. Between December and May, the water samples were
244 undersaturated for calcite and dolomite (October to May for aragonite) and supersaturated
245 between June and November (or September for aragonite).
246

5 – Discussion

5.1 Relative contribution to the dissolved Li load

It is generally agreed that dissolved Li in most of the world's major rivers comes from silicate weathering, and that the fraction derived from carbonate rocks or evaporite is negligible (e.g., Kisakűrek et al., 2005; Gou et al., 2019; Murphy et al., 2019; Martin et al., 2020). In addition, atmospheric deposition from cyclic salts plays a very minor role in the dissolved Li budget (Dellinger et al., 2015; Song et al., 2021). To overcome this input on the Ebro Basin, we corrected only for marine aerosols using the characteristics of modern seawater

The Li concentration from atmospheric input is given by multiplying the Cl concentration from rainwater by the Li/Cl ratio in seawater (Négrel et al., 1993; Dellinger et al., 2015). With a maximum estimated chlorine concentration of 85 μmol L^{-1} deriving from marine input (Avilla and Alarcon, 1999), and a seawater Li/Cl ratio of $5x10^{-5}$ (Millot et al., 2010a), the calculated Li input from rain is low, with a maximum estimated contribution of rainwater-derived Li in the Ebro Basin of 0.04-0.20% for the main tributaries, 0.10-0.40% for the Ebro, and 0.09–0.20% for the outlet. In the Ebro Basin, due to its geological framework, the contribution of carbonate and evaporite dissolution to the dissolved load should be the major input, while the one from silicate can be ignored (Négrel et al., 2007; 2021; Petelet-Giraud and Négrel, 2010).

Figure 3 shows the binary plots between chemical elements in Ebro water, Li is compared to Cl (Fig. 3a) and SO_4 (Fig. 3b). The dissolved load of the Ebro basin (tributaries, main channel, outlet and groundwater) is clearly controlled by gypsum/anhydrite and halite dissolution; few or none of the samples are close to the seawater dilution line regardless of the concentrations (Ega and GA2 groundwater (16, Fig. 1). As can be seen in Figures 3, two main evolution trends explaining most of the Ebro Basin samples, namely the halite-dissolution and

gypsum/anhydrite -evolution lines, respectively constrained by variations in Cl and in SO_4 concentration.

In the Cl *vs.* Li plot (Fig. 3a), the gypsum/anhydrite -evolution line explains the sample values in the Matarrana, Segre and Guadalope tributaries. The halite-dissolution line explains the Aragon, Ega and Gallego tributaries, as well as the samples from the Ebro at 103 km and 241 km from the river source, several outlet results, and groundwater GA15. The rest of the samples plot between these two trends. In the SO_4 *vs.* Li plot (Fig. 3b), the gypsum/anhydrite -evolution line explains the Gallego, Huerva, Segre and Guadalope tributaries, the Ebro sample at 103 km and 241 km from the river source, and groundwater GA15. The halite-dissolution line explains the Matarrana, Ega, Aragon and Cinca tributaries, the Ebro samples at 281 km, 336 km and 543 km from the source, and all samples from the outlet surveys.

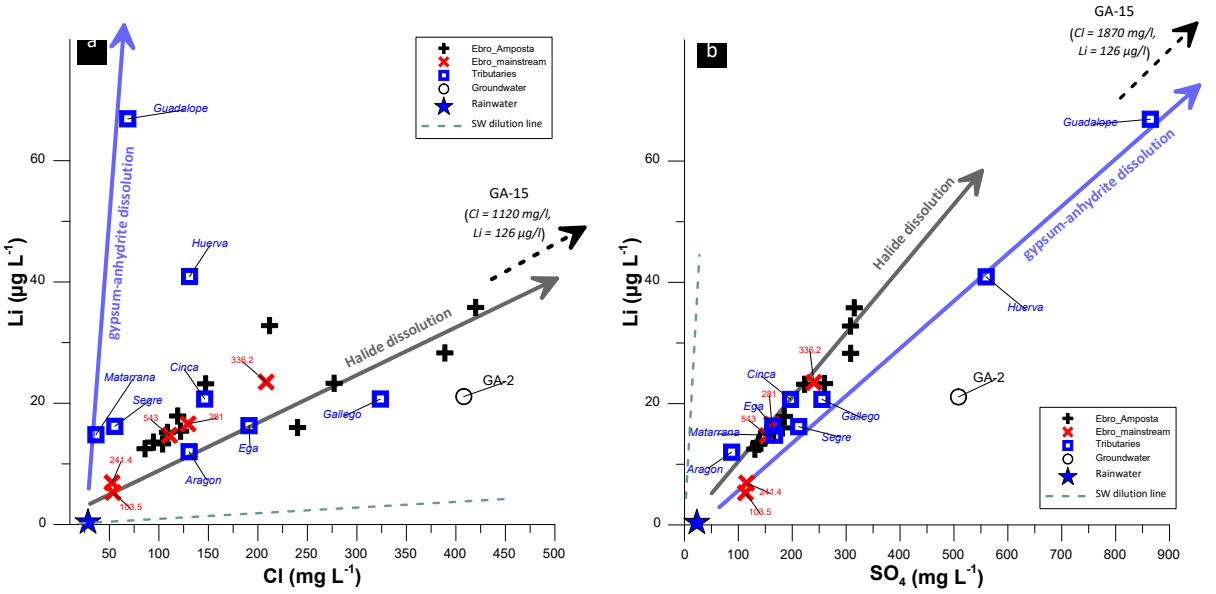

Figure 3. Data from the Ebro Basin regarding tributaries, main channel, outlet and groundwater for concentrations of (a) Cl vs. Li, and (b) SO_4 vs. Li (all values in µg L^{-1}).

The distribution along the two main evolution lines confirms that evaporite weathering plays an important role in controlling Li concentrations, as shown for Cl–SO_4 (Négrel et al.,

2007; Petelet-Giraud and Négrel, 2010). This is in agreement with Isidoro and Aragüés, (2007) who argue that the salinity of water in the Ebro basin originates from three major sources, associated with three minerals, namely gypsum/anhydrite, halite and calcite. Regarding a possible anthropogenic control on Li concentrations, in addition to bedrock sources of dissolved chloride-sulphate, the streams in the Ebro Basin are likely to integrate input from farming and industrial activities. Pollutant investigations have revealed high concentrations near industrial sites for persistent organic pollutants and heavy metal (Bovolo et al., 2011). Among framing impacts, the main pressure on water quality in the Ebro basin is from irrigated areas through the irrigation return flow. The different components of the irrigation return flow are bypass waters, tail-waters and subsurface drainage waters that may be enriched in phosphorous, pesticides, salts and agrochemicals (Aragües and Tanji, 2003) and constitute generally the primary source of pollution. Heavy metal, pesticide and nutrient pollution are widespread in relation to farming activities (pesticides and fertilizers uses).Nitrates fluctuate little, between 4 mg L^{-1} (Gallego) and 19 mg L^{-1} (Huerva) for the maximum range observed in tributaries. Regarding the Ebro itself, the highest NO_3 value (16 mg L^{-1}) is observed at 281 km from the river source, decreasing to 9 mg L^{-1} at 543 km from the source. All outlet survey samples agree with this range of values (6 to 14 mg L^{-1}). No relation is observed between NO_3 and Li concentrations and NO_3 and Cl concentrations, except that the highest NO_3 values correspond to the lowest Li ones. This shows the unrelated behaviour of these elements and the fact that no anthropogenic agricultural or industrial influence on Li can be detected in the Ebro Basin. Even in the two groundwater samples, the high NO_3 concentrations (GA2 = 56 mg L^{-1}, GA15 = 88 mg L^{-1}) are not mirrored by high Li contents, confirming the different origins of Li and NO_3, with a major lithological control for Li.

5.2 Constraints added by Li isotopes: lithological control and fractionation processes

It is now well agreed that δ^7Li values in river waters are higher than in the parent rocks, due to the strong fractionation between the ^{7}Li and ^{6}Li isotopes during weathering (e.g., Huh et al., 1998; 2001; Pistiner and Henderson, 2003; Kisakurek et al., 2005; Vigier et al., 2008; Millot et al., 2010a; Verney-Carron et al., 2011, Dellinger et al., 2015; Wang et al., 2015; Bagard et al., 2015; Négrel and Millot, 2019; Gou et al., 2019; Steinhoefel et al., 2021). While the ^{6}Li isotope is preferentially retained and incorporated into secondary weathering products such as clays and oxides, the ^{7}Li isotope is enriched in the dissolved load, leading to relatively high δ^7Li values in rivers.

The δ^7Li values are commonly correlated with the Na/Li ratio (Millot et al., 2010; Dellinger et al., 2015; Wang et al., 2015; Négrel et al., 2020) and less with the Cl/Li and SO_4/Li ratios (Liu et al., 2011). Figure 4 plots Na/Li ratios *versus* Cl/Li (4a) and SO_4/Li (4b) ones and, in addition to the halite and gypsum/anhydrite dissolution end-member, we consider here Parker's (1967) carbonate dissolution end-member.

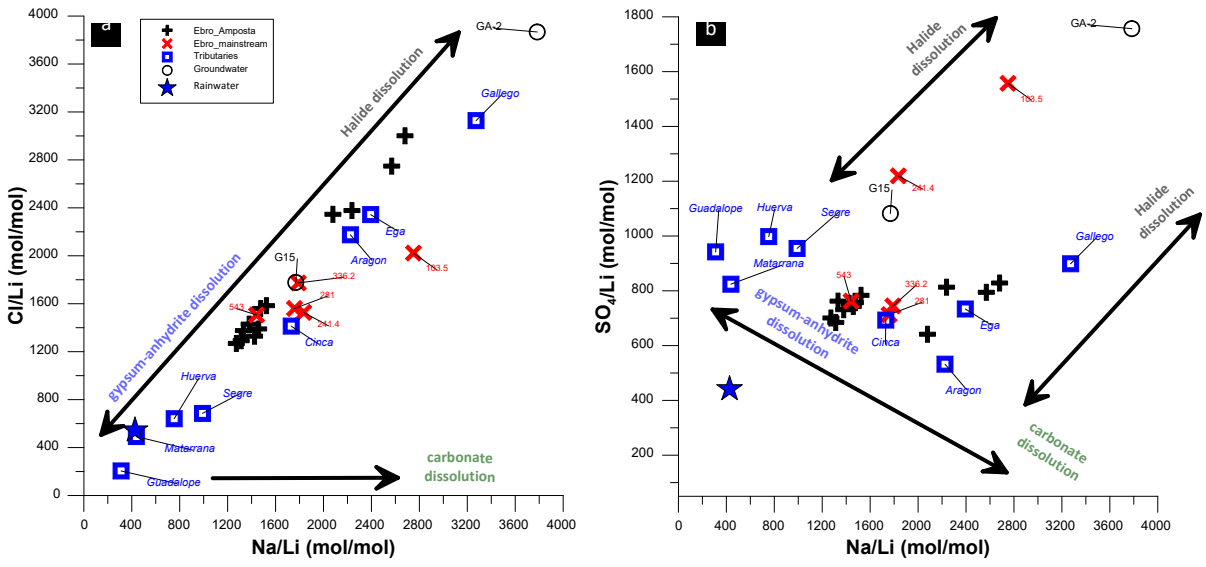

Figure 4. Data from the Ebro Basin concerning tributaries, main channel, outlet and groundwater for concentrations of: (a) Na/Li vs. Cl/Li ratios (in mol/mol), (b) Na/Li vs. SO_4/Li ratios (in mol/mol).

Na/Li *versus* Cl/Li ratios (Fig. 4a) show the role of halite and gypsum/anhydrite psum dissolution, but less that of carbonate. All samples plot along a linear trend with increasing Na/Li and Cl/Li ratios. More precisely than the relationships shown on Figure 3, because concentration effects are reduced when using element ratios, it appears that the Guadalope, Matarrana, Huerva and Segre tributary samples agree with gypsum/anhydrite dissolution, whereas the Gallego, Ega and Aragon ones and GA2 (groundwater) reflect the dissolution of halites. The Ebro samples at 103.5 km from the source appear shifted to the right due to carbonate dissolution, but some samples from the outlet surveys (August to November) are more influenced by halite dissolution when compared to the rest of the survey. The Na/Li *versus* SO_4/Li ratios (Fig. 4b) reflect a more complex behaviour. Guadalope, Matarrana, Huerva and Segre still agree with gypsum/anhydrite dissolution, but Aragon and Cinca for the tributaries, and samples from the Ebro and the outlet show a lowering of SO_4/Li ratios through carbonate dissolution. Gallego and Ega tributary samples and the August to November ones for the outlet are also affected by halite dissolution. Na and Li thus seem to be good indicators of rock-weathering processes in the Ebro Basin, combined as either Na/Li or Li/Na ratios.

It is generally accepted that a positive relationship between the Na/Li molar ratio and the δ^7Li value relates to silicate weathering (Millot et al., 2010; Liu et al., 2011; Dellinger et al., 2015; Wang et al., 2015; Négrel et al., 2020; Steinhoefel et al., 2021), whereas no relationship exists when water is strongly affected by evaporite dissolution (Liu et al., 2011; Wang et al., 2015). In the case of water-evaporite interaction, the Na/Li molar ratio can fluctuate strongly (200 to 550 on the Qinghai-Tibet Plateau; Liu et al., 2011), but less than the variation observed in the Ebro Basin (400 to 3800; Fig. 5a).

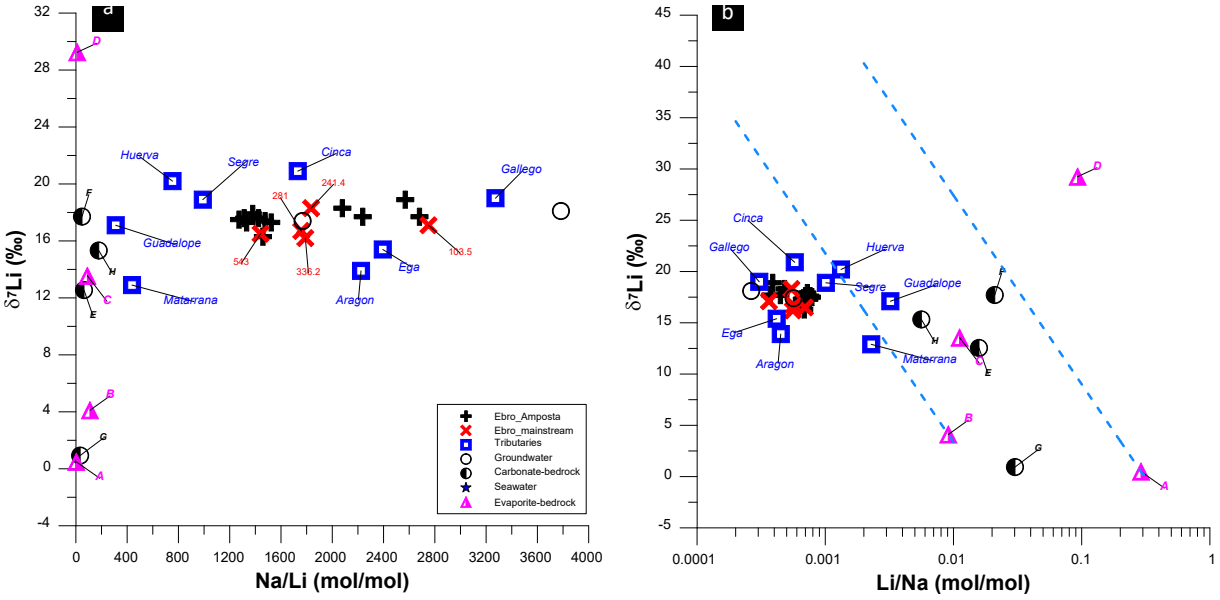

Figure 5. (a) Relationship between dissolved δ^7Li values and molar Na/Li ratios in samples from the Ebro Basin (tributaries, mainstream, outlet, groundwater) and from bedrock. (b) Relationship between dissolved δ^7Li values and molar Li/Na ratios with the simple Rayleigh fractionation model (dotted lines).

Referring to Figure 5, the Segre, Huerva, Matarrana and Guadalope samples are influenced by gypsum/anhydrite dissolution, whereas the Aragon, Gallego and Ega ones show halite-dissolution influence. Thus (Fig. 5a), as these two groups of rivers constitute the extremes of the Na/Li molar-ratio values, the main influence on this ratio is that of the nature of the weathered rocks rather than a fractionation effect (see below). The main feature of Figure 5a is the evidence of two end-members in the tributaries, one marked by gypsum/anhydrite dissolution with low Na/Li molar ratios and the other one marked by halite dissolution with a higher Na/Li molar ratio. Both end-members help explaining the variations observed in the Ebro itself and at the outlet, even if the variations are more marked for the Na/Li molar ratios rather than on the δ^7Li values (Fig. 2a). This scheme reflects a mixing for Li and its isotopes in water being mainly affected by evaporite dissolution, even if the role of carbonate dissolution (less marked in Na concentrations) and a possible influence of Li-

380 isotope fractionation cannot be precluded. The samples collected along the Ebro itself evolve
381 along this mixing scheme. The most upstream value corresponds to an end-member
382 characterized by halite dissolution, and farther downstream the samples are increasingly
383 marked by a component defined by gypsum/anhydrite dissolution. Most of the samples
384 collected at the Ebro outlet can be explained by a component characterized by
385 gypsum/anhydrite dissolution, except for the samples from August to December, with a
386 higher influence of the end-member defined by halite dissolution. Using O and H isotopes,
387 Négrel et al. (2016) showed that from September to November, the Ebro at the outlet is
388 mostly supplied by groundwater and some water retained by dams, as the main river discharge
389 is low. This causes a data shift towards the halite-dissolution end-member, which is well
390 reflected in the groundwater sample that exceeds the Na/Li molar ratio in the Gallego and
391 Cinca waters, reflecting a large influence of evaporite dissolution. This can be due to a double
392 influence of mainly halite dissolution and, secondarily, gypsum/anhydrite dissolution (Figs 2a
393 and 2b) for the E16 groundwater sample from a 7-m-deep irrigation well in Lleida (16,
394 Fig. 1).

395 In order to complete this interpretation, we tentatively applied the simple Rayleigh
396 fractionation model (Fig. 5b) that can describe Li removal from water to secondary phases,
397 using the Li/Na molar ratio and the δ^7Li values (Bagard et al., 2015; Manaka et al., 2017).
398 This model is described by the general equations:

399 $$\delta^7Li_w=\delta^7Li_i+1000(\alpha-1)\ln(f^{Li}_w) \quad \text{(Eq. 1)}$$

400 $$f^{Li}_w=Li/Na_w/Li/Na_i \quad \text{(Eq. 2)}$$

401 where δ^7Li_w and δ^7Li_i are the Li isotope composition of the dissolved phase w and its initial
402 value in the rocks i, α is the fractionation factor, and f^{Li}_w is the Li fraction remaining in the
403 dissolved phase.

However, such a model requires an initial value for calculating the fractionation effect on the Li isotopes. Due to the congruent dissolution of evaporite deposits, we applied Eq. 1 on two initial values representative of the extreme rock end-members, and then examined the Rayleigh fractionation curves obtained by applying Eqs. 1 and 2. These end-members are the two gypsum samples, one from Miocene continental deposits (A in Table 12) with a δ^7Li_i of 0.49 and Li/Na_i of 0.29, and the other from Oligocene continental deposits (B in Table 1) with a δ^7Li_i of 4.11 and Li/Na_i of 0.0091. Values generally used for the fractionation factor α range from 0.996 to 0.993 (Bagard et al., 2015; Manaka et al., 2017)—the latter being accepted for the Ganges, and down to 0.991 for the Amazon River (Dellinger et al., 2015). This range of the fractionation factor α is generally used for silicate weathering studies (Golla et al., 2021), or for large watersheds of varied geology, such as the Ganges or Amazon Basins (Dellinger et al., 2015; Pogge von Strandmann et al., 2021; Yoshimura et al., 2021).

Figure 5b illustrates the relationship between dissolved δ^7Li values and molar Li/Na ratios, with the simple Rayleigh fractionation model from Eqs. 1 and 2. Guadalope plots within the fractionation lines, but Mattarana and Huerva (and Segre to a lesser extent) plot along fractionation line starting from sample B (Oligocene continental deposits). However, most of the δ^7Li values of the water samples in the Ebro plotted away from the fractionation line for α=0.992 chosen on Fig. 5b. This value of 0.992 is close to the α calcite-solution given by Day et al. (2021). It therefore seems confirmed that the Rayleigh fractionation model, as described in Equation 1 and shown on Figure 5b, is not valid in the case of the Ebro. This may be explained by three points. The first concerns the non-removal of Li from water to secondary phases caused by the presence of many dams on the river and its tributaries that trap the suspended load, which is reduced to a few mg/L at Amposta (Négrel et al., 2007) precluding this process. The second explanation concerns the impossibility of applying a fractionation model in this particular case, which may be due to the fact that i) the model was

generally applied in rivers draining silicates (Kisakurek et al., 2005; Millot et al., 2010a; Dellinger et al., 2014; 2015), and that ii) the derived α values were defined under specific weathering conditions or in laboratory experiments, but not under evaporite and carbonate weathering (Song et al;, 2021). The third explanation concerns another process that can control Li at the Ebro Basin scale: in the limestone-evaporite dominated rivers from the Ebro Basin, we have modelled the Sr isotopes as a mixture between carbonate and evaporite endmembers that cover the variability of all samples from the Ebro Basin (Négrel et al., 2021). This reinforces the major role of mixing processes in the Ebro Basin rather than fractionation processes, previously reported and discussed for silicate rocks.

5.3 Coupling Li and Sr isotopes: lithological control and mixing processes

Several studies (Phan et al., 2016; Manaka et al., 2017) have shown that δ^7Li combined with $^{87}Sr/^{86}Sr$ isotopes has the potential of distinguishing between the different rock types subject to weathering, or of explaining mixing processes (Henrichi et al., 2016; Li et al., 2020). Sr isotopes are a robust tracer of mixing because these isotopes do not fractionate (Millot et al., 2011) and combine with Li when the effects of weathering (and/or mixing) supplant those of the fractionation between water and secondary phases (Schmitt et al., 2012). Figure 6a illustrates the relationship between δ^7Li values and $^{87}Sr/^{86}Sr$ ratios in the dissolved load from the Ebro Basin and the various carbonate and evaporite bedrocks. We first note that the Li and Sr isotopes are scattered in the different bedrocks, whose three apexes are the carbonates G (continental Paleocene) and H (Oligocene carbonate), and the evaporite D (Trias anhydrite). Furthermore, all water samples collected in the Ebro Basin lie within the area defined by the bedrocks and define a positive trend (grey arrow on Fig. 6a). Negrel et al. (2021) found that the Sr-isotope levels in the Aragon, Ega, Matarrana and Guadalope samples are explained by a mixing scheme that is mainly influenced by evaporite weathering (gypsum/anhydrite and

halite), whereas the Huerva, Gallego, Cinca and Segre samples show a shared role of evaporite (halites) and carbonate weathering.

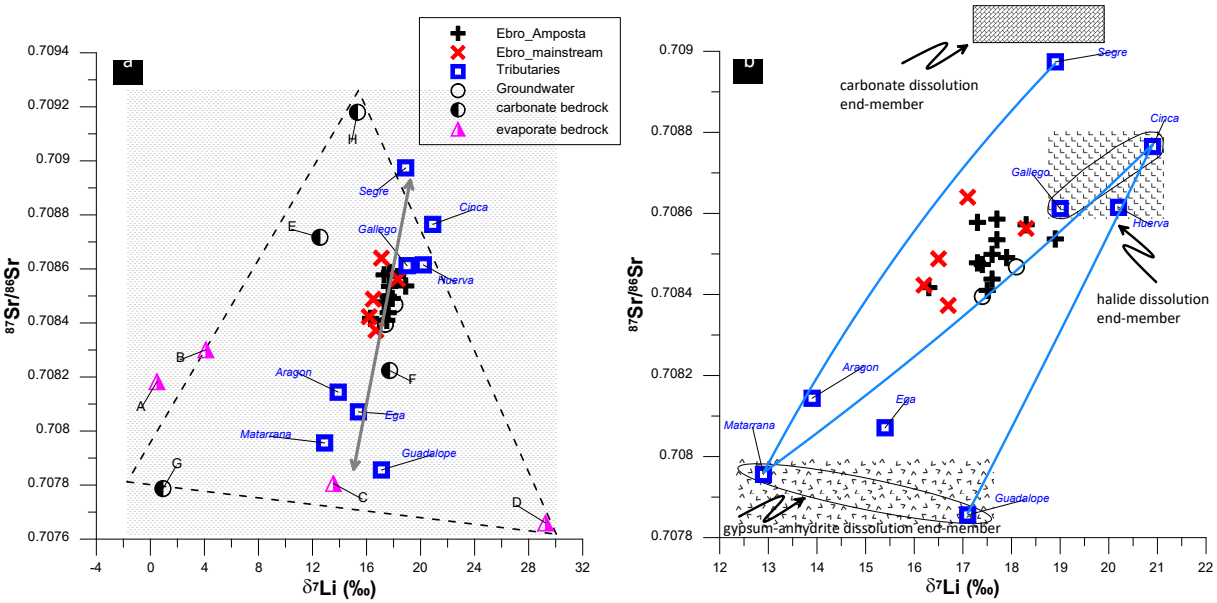

Figure 6. a - Relationship between dissolved δ^7Li values and $^{87}Sr/^{86}Sr$ ratios in the samples from the Ebro Basin (tributaries, mainstream, outlet, groundwater) and bedrock (A to H, Table 1).
b - Extended view of the relationship between the δ^7Li values and $^{87}Sr/^{86}Sr$ ratios in the Ebro basin samples. The carbonate end-member is from Négrel et al., 2021 and this study). Solid lines show theoretical mixtures between the different end-members.

The relationships between several end-members in Figure 6a are represented by hyperbolae (Langmuir et al., 1978; Négrel et al., 2010) and can be expressed as by equation 3, below, I_{mix} being the isotope composition of the mixed solution:

$$I_{mix} = \{([\ ]_a \times I_a \times m)/([\ ]_{mix})\} + \{([\ ]_b \times I_b \times (1- m))/[\ ]_{mix}\} \quad \text{(Eq. 3)}$$

where $[\ ]_a$, $[\ ]_b$ and $[\ ]_{mix}$ are the Li or Sr concentrations for the solution mix from two end-members a and b, I_a, I_b and I_{mix} are the Li or Sr isotope compositions or value for the solution mix from two end-members a and b, and m is the mixing proportion.

Figure 6b shows the relationships between the δ^7Li values and the $^{87}Sr/^{86}Sr$ ratios, and the mixtures between different end-members are represented by curves according to Eq. 3.

Considering only mixing processes, all samples are explained by mixing lines with different end-members, here represented by the Matarrana and Guadalope samples for the gypsum/anhydrite dissolution end-member, and by the Cinca and Gallego ones for the halite dissolution end-member (Figs. 4 and 5). Négrel et al. (2021) found that the Segre water is strongly influenced by carbonate dissolution, and was therefore selected to represent this end-member. Mixtures between Matarrana-plus-Segre and Guadalope-plus-Cinca (and a mixture between Matarrana and Cinca) explain all Li-Sr relationships in the Ebro Basin samples. This mixing scheme again illustrates the major role of evaporite dissolution on Li isotopes, with a non-negligible role of carbonate dissolution, generally considered to be weak in controlling the lithium cycle in watersheds (Kisakurek et al., 2005; Wang et al., 2015).

6 – Conclusions

The Ebro River Basin is the largest catchment of the Iberian Peninsula and one of the largest in the Mediterranean region. Investigations of surface waters and groundwaters defined a detailed behaviour of Li isotopes in the weathering environment at catchment scale. In the rivers dominated by limestone-evaporite bedrock, the waters are isotopically in accordance with the bedrock for their δ^7Li signatures.

Li, Cl and SO_4 concentrations show that they are controlled by evaporite weathering, and that a possible anthropogenic agricultural or industrial influence on Li concentrations can be discarded. The Na/Li, δ^7Li, Cl/Li and SO_4/Li ratios reflect the role of halite dissolution for some tributaries, gypsum/anhydrite dissolution dominates others, but the role of carbonate weathering is minor. Samples from the Ebro main channel and from the outlet logically showed a mix of waters.

Application of the Rayleigh fractionation model cannot explain the observed data. This fact reinforces the major role of mixing processes in the Ebro Basin as fractionation cannot explain the mineral concentrations in most samples. The mixing model is further confirmed by comparison of δ^7Li values and $^{87}Sr/^{86}Sr$ ratios.

Compared with results from other large basins, such as the Amazon, Congo and Ganges-Brahmaputra ones, as well as with data from much smaller catchments and even soil profiles, our study confirms that lithium isotopes are a powerful tool for tracing basin evolution, through different weathering regimes, relief and climate conditions observed in various bedrock-types catchments, including carbonate-evaporite-dominated catchments.

Acknowledgement

This work was funded by the BRGM Research Division and by the European Union (integrated project AquaTerra, Project GOCE 505428) under the thematic priority "Sustainable Development, Global Change and Ecosystems (FP6) Water Cycle and Soil Related Aspects". The views expressed are purely those of the writers and may not under any circumstances be regarded as stating an official position of the European Commission. We thank M. Brach for collecting the samples along the Ebro basin and D. Barcelo's team (CSIC Barcelona, Spain) for assisting in sample collection. We are grateful to Dr. Laura Rosell, Dr. Federico Orti and Dr. Lluis Cabrera for providing the bedrock samples. The authors acknowledge the support on the information received from the Agencia Catalana de l'Aigua and the Confederación Hidrográfica del Ebro (CHE). We are grateful to Dr. H.M. Kluijver for proofreading and editing the English text.

References

Avilla, A., Alarcon, M., 1999. Relationship between precipitation chemistry and meteorological situations at a rural site in NE Spain. Atmospheric Environment 33, 1663–1677.

Aragües, R., Tanji, K.K., 2003 Water quality of irrigation return flows, in: B.A. Stewart & T.A. Howell (Eds). Encyclopaedia of Water Science, pp. 502–506 (New York: Marcel Dekker Inc).

526 Bagard, M.L., West, A.J., Newman K., Basu, A.R., 2015. Lithium isotope fractionation in the Ganges-
527 Brahmaputra floodplain and implications for groundwater impact on seawater isotopic
528 composition. Earth Planet. Sci. Lett. 432, 404–414.
529 Batalla, R.J., Gomez, C.M., Kondolf, G.M., 2004. Reservoir-induced hydrological changes in the Ebro
530 River Basin, NE Spain. J. Hydrol. 290, 117–136.
531 Birnbaum S.J., Coleman M., 1979. Source of sulfur in the Ebro Basin (Northern Spain) Tertiary
532 nonmarine evaporite deposits as evidenced by sulfur isotopes. Chem. Geol. 25, 163-168.
533 Bovolo, C.I., Blenkinsop, S., Majone, B., Zambrano-Bigiarini, M., Fowler, H.J., Bellin, A., Burton,
534 A., Barceló, D., Grathwohl, P. Barth J.A.C. 2011. Climate change, water resources and pollution
535 in the Ebro Basin: Towards an integrated approach. The Ebro River Basin, 295-329.
536 Burton, K.W., Vigier, N. 2011, Lithium isotopes as tracers in marine and terrestrial environments, in
537 Handbook of Environmental Isotope Geochemistry, pp. 41–59, Springer, Berlin Heidelberg.
538 Caritat, P. de, Reimann, C., the NGSA Team, and GEMAS team. 2012. Comparing results from two
539 continental geochemical surveys to world soil composition and deriving Predicted Empirical
540 Global Soil (PEGS2) reference values. Earth Planet. Sci. Lett. 319–320, 269-276.
541 Castillo Herrador, F., 1974. Le Trias évaporitique des bassins de la Vallée de l'Ebre et de Cuenca.
542 Bull. Soc. Géo. Fr. 16, 666-675.
543 CHE. Plan Hidrológico de la cuenca del Ebro. http://oph.chebro.es/PlanHidrologico/inicio.htm, 1996.
544 Choi H.B., Ryu J.S., Shin W.J., Vigier N., 2019. The impact of anthropogenic inputs on lithium
545 content in river and tap water. Nature Communications 10:5371.
546 Cruzado, A., Zoila Velasquez, Z., del Carmen Perez, M., Bahamon, N., Grimaldo N.S., Ridolfi, F.,
547 2002. Nutrient fluxes from the Ebro River and subsequent across-shelf dispersion. Continent. Shelf
548 Res. 22, 349–360.
549 Day, C.C., Pogge von Strandmann, P.A.E., Mason, A.J. 2021. Lithium isotopes and partition
550 coefficients in inorganic carbonates: Proxy calibration for weathering reconstruction. Geochim.
551 Cosmochim. Acta 305, 243-262.
552 Dellinger, M., Gaillardet, J., Bouchez, J., Calmels, D., Galy, V., Hilton, R.G., Louvat, P., France-
553 Lanord, C., 2014. Lithium isotopes in large rivers reveal the cannibalistic nature of modern
554 continental weathering and erosion. Earth Planet. Sci. Let. 401, 359-372.
555 Dellinger, M., Gaillardet, J., Bouchez, J., Calmels, D., Louvat, P., Dosseto, A., Gorge, C., Alanoca, L.,
556 Maurice, L., 2015. Riverine Li isotope fractionation in the Amazon River basin controlled by the
557 weathering regimes. Geochim. Cosmochim. Acta 164, 71–93.
558 Elorza M.G., Santolalla F.G., 1998. Geomorphology of the Tertiary gypsum formations in the Ebro
559 Depression (Spain). Geoderma 87, 1-29.
560 Farber, E., Vengosh, A., Gavrieli, I., Marie, A., Bullen, T. D., Mayer, B., Holtzman, R., Segal, M.,
561 Shavit, U., 2004. The origin and mechanisms of salinization of the Lower Jordan River. Geochim.
562 Cosmochim. Acta 68, 1989-2006.

Golla, J.K., Kuessner, M.L., Henehan, M.J., Bouchez, J., Rempe, D.M., Druhan, J.L. 2021. The evolution of lithium isotope signatures in fluids draining actively weathering hillslopes. Earth Planet. Sci. Lett. 567, 116988.

Gou, L.F., Jin, Z., Pogge von Strandmann, P.A.E., Li, G., Qu, Y.X., Xiao, J., Deng, L., Galy, A., 2019. Li isotopes in the middle Yellow River: Seasonal variability, sources and fractionation. Geochim. Cosmochim. Acta 248, 88-108.

Guillen, J., Palanques, A., 1992. Sediment dynamics and hydrodynamics in the lower course of a river highly regulated by dams: the Ebro River. Sediment. 39, 567–579.

Ibáñez, C., Prat, N., Cancio, A., 1996. Changes in the hydrology and sediment transport produced by large dams on the lower Ebro River and its estuary. Regul. Riv. 12, 51–62.

INE. Censo Agrario 1999. Instituto Nacional de Estadistica. [CD-ROM], Madrid, 2003.

Isidoro, D., Aragüés, R., 2007. River water quality and irrigated agriculture in the Ebro basin: An overview. Water Resources Development, 23(1), 91-106.

Henchiri, S., Gaillardet, J., Dellinger, M., Bouchez, J., Spencer, R.G.M., 2016. Riverine dissolved lithium isotopic signatures in low-relief central Africa and their link to weathering regimes, Geophys. Res. Lett. 43, doi:10.1002/2016GL067711.

Huh, Y., Chan, L.H., Zhang, L., Edmond, J.M., 1998. Lithium and its isotopes in major world rivers: implications for weathering and the oceanic budget. Geochim. Cosmochim. Acta 622, 2039–2051.

Huh, Y., Chan, L.H., Edmond, J.M., 2001. Lithium isotopes as a probe of weathering processes: Orinoco River. Earth Planet. Sci. Lett. 194, 189–199.

Kisakurek, B., James, R.H., Harris, N.B.W., 2005. Li and δ^7Li in Himalayan rivers: proxies for silicate weathering? Earth Planet. Sci. Lett. 237, 387–401.

Langmuir, C.H., Vocke, R.D., Hanson, G.N., 1978. A general mixing equation with application to Icelandic basalts. Earth Planet. Sci. Lett. 37, 380-392.

Li, W., Liu, X.M., Chadwick, O.A., 2020. Lithium isotope behavior in Hawaiian regoliths: Soil-atmosphere-biosphere exchanges. Geoch. Cosmochim. Acta 285, 175-192.

Liu, C.Q., Zhao, Z.Q., Wang, Q., Gao, B., 2011. Isotope compositions of dissolved lithium in the rivers Jinshajiang, Lancangjiang, and Nujiang: Implications for weathering in Qinghai-Tibet Plateau. Appl. Geochem. 26, S357-S359.

Luzón, A., Pérez, A., Soriano, M.A., Pocoví, A., 2008. Sedimentary record of Pleistocene paleodoline evolution in the Ebro basin (NE Spain). Sedimentary Geology, 205(1-2), 1-13.

Manaka, T., Araoka, D., Yoshimura, T., Hossain, H. Z., Nishio, Y., Suzuki, A., Kawahata, H., 2017. Downstream and seasonal changes of lithium isotope ratios in the Ganges-Brahmaputra river system. Geochem. Geophys. Geosys. 18, 3003-3015.

Martin, A.N., Meredith, K., Norman, M.D., Bryan, E., Baker, A., 2020. Lithium and strontium isotope dynamics in a carbonate island aquifer, Rottnest Island, Western Australia. Sci. Total Environ. 715, 136906.

600 Millot, R., Guerrot, C., Vigier, N., 2004. Accurate and high precision measurement of lithium isotopes
601 in two reference materials by MC-ICP-MS. Geostandards Geoanalytical Res. 28, 153–159.
602 Millot, R., Négrel, Ph., Petelet-Giraud, E., 2007. Multi-isotopic (Li, B, Sr, Nd) approach for
603 geothermal reservoir characterization in the Limagne Basin (Massif Central, France). Appl.
604 Geochem. 22, 2307–2325.
605 Millot, R., Négrel, Ph., 2021. Lithium isotopes in the Loire River Basin (France): hydrogeochemical
606 characterizations at two complementary scales. Appl. Geochem. 125, 104831.
607 Millot, R., Vigier, N., Gaillardet, J., 2010a. Behaviour of lithium and its isotopes during weathering in
608 the Mackenzie Basin, Canada. Geochim. Cosmochim. Acta doi:10.1016/j.gca.2010.04.057.
609 Millot, R., Petelet-Giraud, E., Guerrot, C., Négrel, Ph., 2010b. Multi-isotopic composition (δ^7Li–δ^{11}B–
610 δD–δ^{18}O) of rainwaters in France: Origin and spatio-temporal characterization. Appl. Geochem. 25,
611 1510-1524.
612 Millot, R., Guerrot, C., Innocent, C., Négrel, Ph., Sanjuan, B., 2011. Chemical, multi-isotopic (Li-B-
613 Sr-U-H-O) and thermal characterization of Triassic formation waters from the Paris Basin. Chem.
614 Geol. 283, 226-241.
615 Mochales, T., Pueyo, E.L., Casas, A.M., Soriano, M.A., 2007. Magnetic prospection as an efficient
616 tool for doline detection: a case study in the central Ebro Basin (northern Spain). Geological
617 Society, London, Special Publications, 279(1), 73-84.
618 Murphy, M.J., Porcelli, D., Pogge von Strandmann, P.A.E., Hirst, C.A., Kutscher, L., Katchinoff, J.A.,
619 Mörth, C.M., Maximov, T., Andersson, P.S., 2019. Tracing silicate weathering processes in the
620 permafrost-dominated Lena River watershed using lithium isotopes. Geoch. Cosmochim. Acta
621 245, 154-171.
622 Négrel, Ph., Petelet-Giraud, E., Guerrot, C., Millot, R., 2021. Ca and Sr isotope constraints on
623 chemical weathering processes: A view through the Ebro river basin, Spain. Chem. Geol. 578,
624 120324.
625 Négrel, Ph., Millot, R., Petelet-Giraud, E., Klaver, G., 2020. Li and δ^7Li as proxies for weathering and
626 anthropogenic activities: application to the Dommel River (Meuse basin). Appl. Geochem. 120,
627 104674.
628 Négrel, Ph., Petelet-Giraud, E., Millot, R., 2016. Tracing water cycle in regulated basin using stable
629 δ^{18}O–δ^2H isotopes: The Ebro river basin (Spain). Chem. Geol. 422, 71-81.
630 Négrel, Ph., Roy, S., Petelet-Giraud, E., Millot, R., Brenot, A., 2007. Long-term fluxes of dissolved
631 and suspended matter in the Ebro River Basin (Spain). J. Hydrol. 342, 249-260.
632 Négrel, Ph., Allègre, C.J., Dupré, B., Lewin, E., 1993. Erosion sources determined from inversion of
633 major, trace element values and strontium isotopic values in riverwater: the Congo Basin case.
634 Earth Planet. Sci. Lett. 120, 59–76.

635 Négrel, Ph., Millot, R., 2019. Behaviour of Li isotopes during regolith formation on granite (Massif
636 Central, France): Controls on the dissolved load in water, saprolite, soil and sediment. Chem. Geol.
637 523, 121-132.
638 Négrel, Ph., Millot, R., Brenot, A., Bertin, C., 2010. Lithium isotopes as tracers of groundwater
639 circulation in a peat land. Chem. Geol. 276, 119-127.
640 Négrel, Ph., Millot, R., Guerrot, C., Petelet-Giraud, E., Brenot, A., Malcuit, E., 2012. Heterogeneities
641 and interconnections in groundwaters: Coupled B, Li and stable-isotope variations in a large
642 aquifer system (Eocene Sand aquifer, Southwestern France). Chem. Geol. 296, 83-95.
643 Négrel, Ph., Millot, R., 2019. Behaviour of Li isotopes during regolith formation on granite (Massif
644 Central, France): Controls on the dissolved load in water, saprolite, soil and sediment. Chem.
645 Geol. 523, 121-132.
646 Négrel, Ph., Grosbois, C., 1999. Changes in chemical and $^{87}Sr/^{86}Sr$ signatures distribution patterns of
647 suspended matter and bed sediments in the upper Loire River basin (France). Chem. Geol. 156,
648 231-249.
649 Ortì F., 1990. Introducción a las evaporitas de la Cuenca Terciaria del Ebro. In : Ortì F., Salvany J.M.
650 (Eds.), Formaciones evaporìticas de la Cuenca del Ebro y cadenas peridéricas, y de la zona de
651 Levante. ENRESA-GPPG, Barcelona, pp.62-66.
652 Parkhurst, D.L., Appelo, C.A.J., 1999. User's guide to PHREEQC (Version 2): A computer program
653 for speciation, batch-reaction, one-dimensional transport, and inverse geochemical calculations.
654 Water-Resources Investigations Report 99, 4259, 312pp.
655 Parker, R.L., 1967. Composition of the Earth's crust. U.S. Geological Survey Professional Paper 440-
656 D, 17 pp.
657 Petelet-Giraud, E., Négrel, Ph., 2010. Dissolved fluxes of the Ebro River Basin (Spain): Impact of
658 main lithologies and role of tributaries. In The Ebro River Basin (pp. 97-120). Springer, Berlin,
659 Heidelberg.
660 Phan, T.T., Capo, R.C., Stewart, B.W., Macpherson, G.L., Rowan, E.L., Hammack, R.W., 2016.
661 Factors controlling Li concentration and isotopic composition in formation waters and host rocks
662 of Marcellus Shale, Appalachian Basin. Chem. Geol. 420, 162-179.
663 Pistiner, J.S., Henderson, G.M., 2003. Lithium-isotope fractionation during continental weathering
664 processes. Earth Planet. Sci. Lett. 214, 327–339.
665 Pogge von Strandmann, P.A.E., Burton, K.W., James, R.H., van Calsteren, P. Gíslason, S.R.,
666 Mokadem F., 2006. Riverine behaviour of uranium and lithium isotopes in an actively glaciated
667 basaltic terrain. Earth Planet. Sci. Lett. 251, 134–147.
668 Pogge von Strandmann, P.A.E., Porcelli, D., James, R.H., van Calsteren, P., Schaefer, B., Cartwright,
669 I., Reynolds, B.C., Burton, K.W., 2014. Chemical weathering processes in the Great Artesian
670 Basin: evidence from lithium and silicon isotopes. Earth Planet. Sci. Lett. 406, 24–36.

671 Pogge von Strandmann, P.A.E., Frings, P.J., Murphy, M.J., 2017. Lithium isotope behaviour during
672 weathering in the Ganges Alluvial Plain. Geochim. Cosmochim. Acta 198, 17-31.
673 Pogge von Strandmann, P.A.E., Burton, K.W., Opfergelt, S., Genson, B., Guicharnaud, R.A.,
674 Gislason, S.R. 2021. The lithium isotope response to the variable weathering of soils in Iceland.
675 Geochim. Cosmochim. Acta 313, 55-73.
676 Qi, H., Ma, C., He, Z., Hu, X., Gao, L., 2019. Lithium and its isotopes as tracers of groundwater
677 salinization: a study in the southern coastal plain of Laizhou Bay, China. Sci. Total Environ. 650,
678 878-890.
679 Rudnick, R.L., Tomascak, P.B., Njo, H.B., Gardner, L.R., 2004. Extreme lithium isotopic
680 fractionation during continental weathering revealed in saprolites from South Carolina. Chem.
681 Geol. 212, 45–57.
682 Schmitt, A.D., Vigier, N., Lemarchand, D., Millot, R., Stille, P., Chabaux, F., 2012. Processes
683 controlling the stable isotope compositions of Li, B, Mg and Ca in plants, soils and waters: A
684 review. Comptes Rendus Geoscience, 344(11-12), 704-722.
685 Song, Y., Zhang, X. Y., Bouchez, J., Chetelat, B., Gaillardet, J., Chen, J., Zhang, T., Cai, H. Yuan, W.,
686 Wang, Z. 2021. Deciphering the signatures of weathering and erosion processes and the effects of
687 river management on Li isotopes in the subtropical Pearl River basin. Geochim. Cosmochim. Acta
688 313, 340-358.
689 Steinhoefel, G., Brantley, S.L., Fantle, M.S., 2021. Lithium isotopic fractionation during weathering
690 and erosion of shale. Geochim. Cosmochim. Acta 295, 155-177.
691 Utrilla R., Pierre C., Ortì F., Pueyo J.J., 1992. Oxygen and sulfur isotope compositions as indicators of
692 the origin of Mesozoic and Cenozoic evaporites from Spain. Chem. Geol. 102, 229-244.
693 Verney-Carron, A., Vigier, N., Millot, R., 2011. Experimental determination of the role of diffusion on
694 Li isotope fractionation during basaltic glass weathering. Geochim. Cosmochim. Acta 75, 3452–
695 3468.
696 Vigier, N., Decarreau, A., Millot, R., Carignan, J., Petit, S., France-Lanord, C., 2008. Quantifying Li
697 isotope fractionation during smectite formation and implications for the Li cycle. Geochim.
698 Cosmochim. Acta 72, 780–792.
699 Wang, Q.L., Chetelat, B., Zhao, Z.Q., Ding, H., Li, S.L., Wang, B.L., Li, J., Liu, X.L., 2015. Behavior
700 of lithium isotopes in the Changjiang River system: sources effects and response to weathering and
701 erosion. Geochim. Cosmochim. Acta 151, 117–132.
702 Yoshimura, T., Araoka, D., Kawahata, H., Hossain, H.M.Z., Ohkouchi, N. 2021. The influence of
703 weathering, water sources, and hydrological cycles on lithium isotopic compositions in river water
704 and groundwater of the Ganges–Brahmaputra–Meghna river system in Bangladesh. Front. Earth
705 Sci. 9: 668757.